Article:

Regulating the morphology of fluorinated non-fullerene acceptor and polymer donor via binary solvent mixture for high efficiency polymer solar cells

Mengxue Chen[a,b+], Zhuohan Zhang[c+], Wei Li[a,b], Jinlong Cai[a,b], Jiangsheng Yu[c], Emma L. K. Spooner[d], Rachel C. Kilbride[d], Donghui Li[a,b], Baocai Du[a,b], Robert S. Gurney[a,b], Dan Liu[a,b], Weihua Tang[c], David G. Lidzey[d], Tao Wang[a,b,*]

[a] School of Materials Science and Engineering, Wuhan University of Technology, Wuhan 430070, China   E-mail: twang@whut.edu.cn

[b] State Key Laboratory of Silicate Materials for Architectures, Wuhan University of Technology, Wuhan 430070, China

[c] School of Chemical Engineering, Nanjing University of Science and Technology, Nanjing 210094, China

[d] Department of Physics and Astronomy, University of Sheffield, Sheffield, S3 7RH, UK

[+] These authors contribute equally to the work.

Abstract: Fluorinated non-fullerene acceptors (NFAs) usually have planar backbone and a higher tendency to crystallize compared to their non-fluorinated counterparts, which leads to enhanced charge mobility in organic solar cells (OSCs). However, this self-organization behavior may result in excessive phase separation with electron donors and thereby deteriorate device efficiency. Herein, we demonstrate an effective approach to tune the molecular organization of a fluorinated NFA (INPIC-4F), and its phase separation with the donor PBDB-T, by varying the casting solvent. A prolonged film drying time encourages the crystallization of INPIC-4F into spherulites and consequently results in excessive phase separation, leading to a low device *PCE* of 8.1%. Contrarily, a drying time leads to fine mixed domains with inefficient charge transport properties, resulting in a moderate device *PCE* of 11.4%. An intermediate film drying time results in the formation of face-on π–π stacked PBDB-T and INPIC-4F domains with continuous phase-separated networks, which facilitates light absorption, exciton dissociation as well as balanced charge transport towards the electrode, and achieves a remarkable *PCE* of 13.1%. This work provides a rational guide for optimizing the molecular ordering of NFAs and electron donors for high device efficiency.

Key words: organic solar cells, non-fullerene acceptors, solvent, morphology, efficiency

Introduction

In the past few years the tremendous progress of solution processed organic solar cells (OSCs) have been exemplified by the use of non-fullerene electron acceptors (NFAs).[1-7] Impressively, non-fullerene OSCs with a bulk heterojunction (BHJ) photoactive layer have demonstrated a maximum power conversion efficiency (PCE_{max}) over 16%,[8] showing their encouraging potential as a green energy resource. In comparison to traditional fullerene acceptors, NFAs show a multitude of advantages including tunable energy levels, strong absorption in the visible and near-infrared region, as well as high carrier mobility.[9-11] Among the reported NFAs in the literature, acceptor-donor-acceptor (A-D-A) type small molecules based on electron-donating fused aromatic cores coupled with strong electron-accepting end groups,[12-14] such as ITIC,[15] have attracted considerable attention for their outstanding optoelectronic performance. For example, an efficient ITIC-based OSC employing a medium bandgap polymer PBDB-T as the donor has achieved a high *PCE* of 11.2%.[16]

To further improve the efficiency of non-fullerene OSCs, a variety of molecular design strategies have been utilized such as side chain engineering,[17-19] donor-acceptor structure modification[20] and functional moiety modulation.[21, 22] Among these methods, introducing fluorine (F) atoms into NFAs has been widely investigated.[23-25] With a small Van der Waals radius and large electronegativity, the F atom improves molecular planarity and aggregation, as well as increasing crystallization tendency due to the noncovalent interactions between sulfur (S) and hydrogen (H) atoms.[26] In addition, fluorination down-shifts both the highest occupied molecular orbital (HOMO) and the lowest unoccupied molecular orbital (LUMO) levels, resulting in narrower bandgap and thus broadened absorption spectrum.[27, 28] For example, Hou et al. reported a fluorinated NFA, IT-4F, whose high-performance was achieved by introducing F atom to the end-groups of ITIC. Compared with its counterpart, IT-4F shows a reduced optical bandgap and down-shifted energy levels. As a result, the IT-4F-based OSCs delivered a maximum *PCE* of 13.1% with PBDB-T-SF as the donor and 13.5% with PM6 as the donor.[29, 30] Hou et al. also reported another novel A-D-A structured NFA named IEICO-4F, by introducing F atoms in IEICO's A moieties. The absorption spectrum of IEICO-4F was redshifted approximately 110 nm with an ultra-narrow bandgap of 1.2 eV. When blended with donors PBT7-Th and J52, the PCE of IEICO-4F-based ternary OSCs reached 10.9%.[31-33] However, the tendency of fluorinated NFAs to organize increases their crystallinity,

which has been found to induce excessive phase separation within a rough photoactive layer which compromises their benefit to OSCs.[26, 28]

In this work, we demonstrate the ability to control the molecular ordering of a fluorinated NFA INPIC-4F by varying the casting solvent, and in doing so regulating the phase-separated morphology in its photovoltaic blends with the electron-donor PBDB-T. Binary solvent strategy has been used in fullerene based solar cells,[34-37] but hasn't been reported so far in non-fullerene-based solar cells. Solvents of chlorobenzene (CB), chloroform (CF) and their mixtures, which have different boiling points therefore evaporation rate, have been applied to manipulate the film drying time during which molecular organization occurs.[38, 39] Synchrotron-based grazing incidence wide-angle X-ray scattering (GIWAXS) and surface morphology characterization have been applied to investigate the molecular order of PBDB-T and INPIC-4F films developed with different solution casting processes. We find that an intermediate film drying process, employing a CB:CF mixture (1.5:1, v/v) as the casting solvent, suppresses the crystallization of INPIC-4F and encourages the formation of face-on $\pi-\pi$ stacked PBDB-T and INPIC-4F molecules, which facilitates light absorption, exciton dissociation as well as balanced charge transport towards the electrode, and achieves a remarkable maximum *PCE* of 13.1%. This work provides a rational guide for optimizing the molecular ordering of fluorinated NFAs with their electron donors for high device efficiency.

Results and Discussion

The chemical structures of PBDB-T and INPIC-4F studied in this work are shown in **Figure 1a**. PBDB-T has been demonstrated to be an effective electron donor for preparing high performance OSCs together with a variety of NFAs.[40, 41] The fluorination of NFA molecule INPIC to INPIC-4F improves the planarity of the molecular backbone and its tendency to self-organize into ordered structure, exhibiting a high electron mobility. As described in **Figure 1b**, the HOMO/LUMO levels of PBDB-T and INPIC-4F were determined to be -5.21/-3.67 eV and -5.42/-3.94 eV.[42, 43] Moreover, the low-lying HOMO/LUMO levels may have certain advantages, such as good stability and large polarization, which is beneficial to OSC devices. We fabricated OSC devices with an inverted structure to investigate the photovoltaic performance. Solvents CB (boiling point of 132 °C), CF (boiling point of 62 °C), and CB/CF mixtures are employed to vary the film drying time during the spin-coating process and thus control the molecular organization of PBDB-T and INPIC-4F to impact device performance. Here, films casting using CF dry much faster

than those cast from CB, which therefore kinetically suppressed the molecular organization of donors and acceptors during the solution casting process. Previous work has shown that the addition of 1,8-diiodooctane (DIO) (0.5 vol%) into the casting solvent CB and a succedent thermal annealing (TA, 100 °C, 10min) help to improve the performance of PBDB-T:INPIC-4F solar cells.[42] Our device study in this work also confirmed that DIO and TA treatments delivered better device efficiency (see **Table S1**), and we therefore adopted this recipe but varied the primary solvent using CB, CF and CB/CF mixture to evaluate the effect of casting solvent on morphology and device performance.
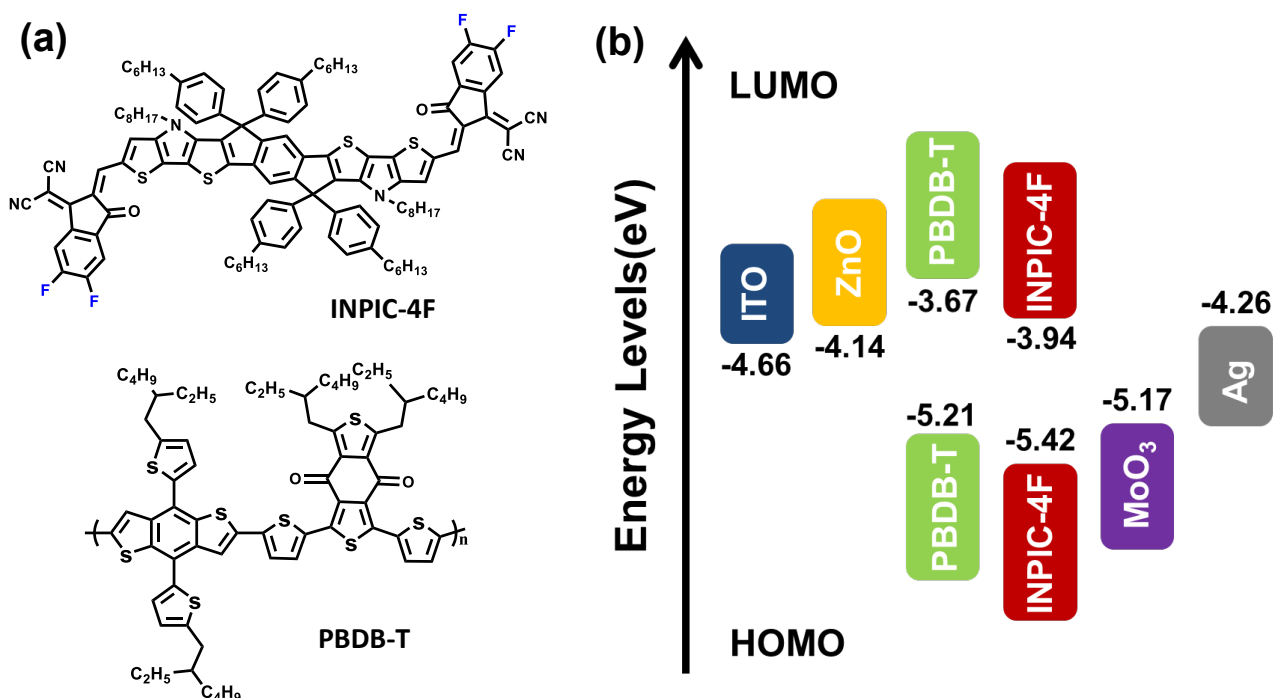

Figure 1 (a) Chemical structures of INPIC-4F and PBDB-T. (b) Energy level diagrams of ITO/ZnO/PBDB-T:INPIC-4F/MoO$_3$/Ag inverted devices.

The J-V curves of our best-performing OSCs with the photoactive layer cast using different solvents are displayed in **Figure 2a**, with the device metrics summarized in **Table 1**. When the conventionally-used CB was employed as the casting solvent, the device gave a poor maximum *PCE* (*PCE$_{max}$*) of 8.1%, with a fill-factor (*FF*) of 66.5%, short-circuit current density (*J$_{sc}$*) of 14.6 mA cm^{-2} and open-circuit voltage (*V$_{oc}$*) of 0.84 V. These values are close to our previous report when the CB-based photovoltaic solution was cast onto device substrate held at room temperature.[44] When the casting solvent was CF, the resulting device had a *PCE$_{max}$* of 11.4%, with a *FF* of 72.2%, *J$_{sc}$* of 19.1 mA cm^{-2} and *V$_{oc}$* of 0.83 V. Binary solvent mixtures of CB and CF (at

4

volume ratios of 2:1, 1.5:1 and 1:1) were also chosen as casting solvents to prepare the photoactive layer, and the device J-V curves are plotted in **Figure S1a** with device data summarized in **Table S2**. It can be seen that when the CB:CF ratio was 1:1 and 1.5:1, both average and maximum device *PCEs* were improved compared with those of the CF-cast device. The best *PCEmax* of 13.1% was recorded with a *FF* of 72.7%, J_{sc} of 22.0 mA cm^{-2} and V_{oc} of 0.82 V when the CB:CF volume ratio was 1.5:1. To verify the accuracy of the J-V measurements, the corresponding external quantum efficiencies (*EQE*) of devices were measured and are shown in **Figure 2b**. The *EQE* curves illustrate that the OSC devices have a broad response in the wavelength range from 300 to 920 nm. When CB was explored as the casting solvent, the EQE value is lower than 60% in the wavelength range from 300 to 900 nm, which is associated with the excessive crystal domain size of INPIC-4F. The maximum EQE value reaches 68% when CF was the casting solvent, and reaches 76% when the CB:CF volume ratio is 1.5:1. The J_{sc} values integrated from the EQE spectra are summarized in **Table 1**. These calculated J$_{sc}$ are only *ca.* 5% less than the J_{sc} values obtained from our J-V scans, therefore confirming the validity of our J-V measurements. These results indicate that a proper drying time during the spin-coating process will significantly affect device performance.
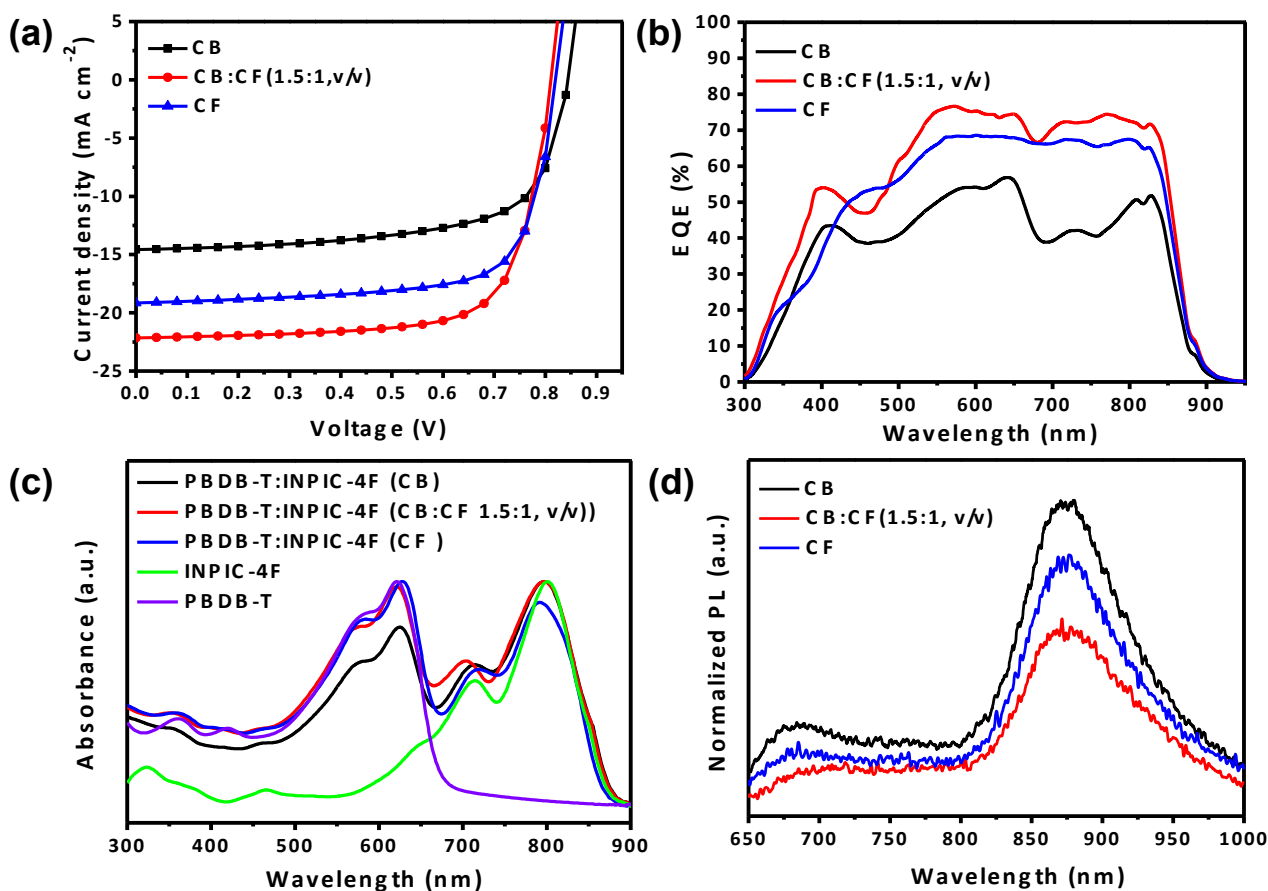
Figure 2 (a) *J-V* characteristics, (b) *EQE* of PBDB-T:INPIC-4F solar cells cast using different solvents. (c) Absorbance and (d) *PL* spectra of PBDB-T:INPIC-4F films cast using different solvents.

Table 1 Photovoltaic parameters of PBDB-T:INPIC-4F OSCs measured at an illumination of AM 1.5 G, 100 mW cm^{-2}. The statistical data were obtained from over 25 individual devices.

Solvent	FF [%]	J_{sc} [mA cm^{-2}]	Calculated J_{sc} [mA cm^{-2}]	V_{oc} [V]	PCE_{max} (PCE_{avg}) [%]
CB	66.5	14.6	14.0	0.84	8.1 (7.4±0.9)
CB:CF(1.5:1, v/v)	72.7	22.0	21.4	0.82	13.1 (12.9±0.3)
CF	72.2	19.1	18.5	0.83	11.4 (11.0±0.5)

The absorption spectra of these films are presented in **Figure 2c**. The pure PBDB-T film displays a primary absorption peak at 621 nm, and low absorption at wavelengths over 700 nm. The INPIC-4F film shows the strongest absorption at 802 nm, whilst its absorption in the wavelength region below 600 nm is relatively weak. For PBDB-T:INPIC-4F blend films, the absorption from 500 to 700 nm can be mainly attributed to PBDB-T and the absorption from 700 to 900 nm can be ascribed to INPIC-4F. When CB was employed as the casting solvent, the photoactive film has the longest time to dry and INPIC-4F had sufficient time to self-organize, which enhanced the absorption over the long wavelength range. Contrastingly, the absorption of PBDB-T in the short wavelength range from 400 to 700 nm is the lowest by casting from CB (see **Figure 2c**), which we attribute to the disruption of PBDB-T molecular order due to the strong crystallinity of INPIC-4F. Meanwhile, this strong crystallization of INPIC-4F also induced excessive phase separation, which is not ideal for efficient charge dissociation and collection, and consequently led to low *EQE* spectrum intensity (see **Figure 2b**). These molecular ordering and phase separation characteristics will be presented in a later section. When CF was employed as the casting solvent, the absorption in the wavelength range from 400 to 700 nm increased, although the absorption from 700 to 900 nm decreased slightly due to reduced molecular ordering of INPIC-4F as a result of shorter organization time during film drying. The intensity of the *EQE* spectrum increased through the whole wavelength range due to the enhanced absorption as well as the improved morphology benefitting

charge generation. When the solvent mixture CB:CF (1.5:1, v/v) was adopted, both absorption and *EQE* spectra were the strongest, suggesting an optimum morphology for light absorption and charge generation. **Figure 2d** depicts the photoluminescence (*PL*) spectra of the blend films. The primary *PL* peak of the blend stays at 870 nm, but the *PL* intensity was quenched most when the CB:CF (1.5:1, v/v) solvent mixture was used, which indicates that there exists the largest amount of donor/acceptor interfaces for efficient charge transfer in the blend film.
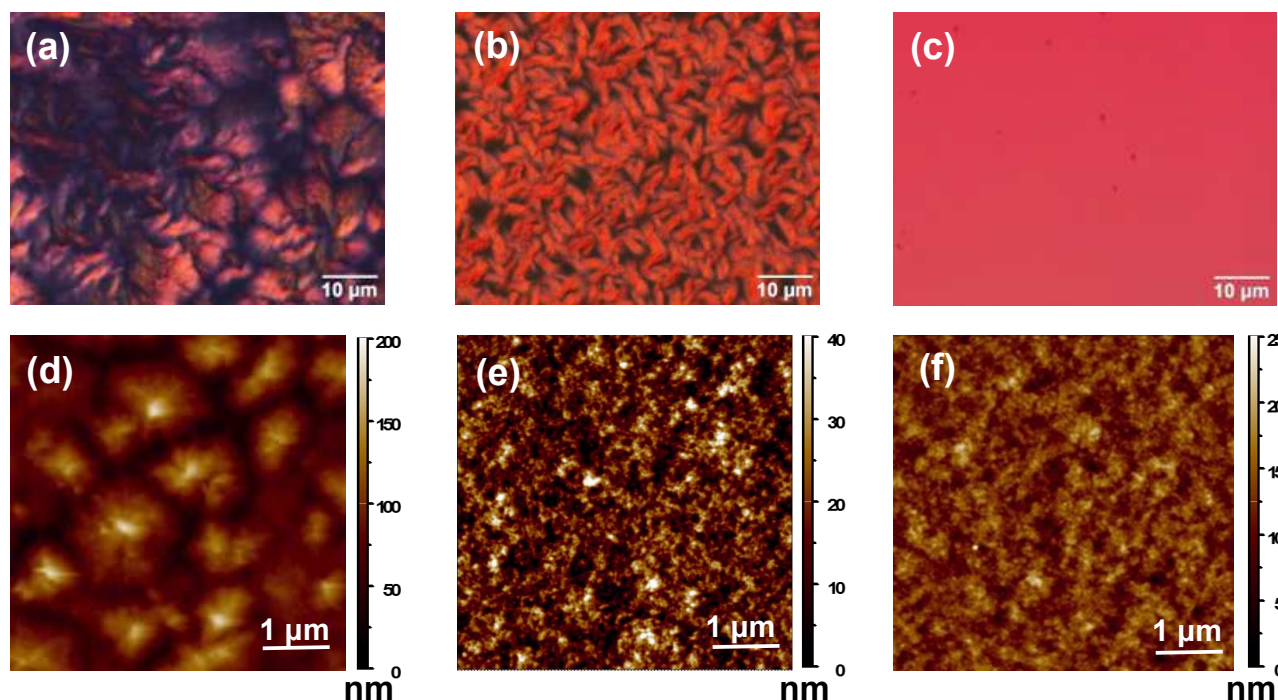

Figure 3 Optical microscope images of INPIC-4F films cast from (a) CB, (b) CB:CF (1.5:1, v/v) and (c) CF. AFM images of PBDB-T:INPIC-4F blend films cast from (d) CB, (e) CB:CF (1.5:1, v/v) and (f) CF.

In order to gain more insight into how the casting solvent will affect the molecular ordering of the INPIC-4F electron-acceptor, we used an optical microscope to observe the morphologies of pure INPIC-4F films cast using different solvents (see **Figure 3a-c**). The film surface was rough when CB was the casting solvent, with the appearance of large crystallites of INPIC-4F. In striking contrast, the film was uniform and smooth when CF was the casting solvent, an effect that we attribute to the least structure order due to the limited organization time during film drying. As expected, when using CB:CF (1.5:1, v/v) mixture as the casting solvent, INPIC-4F has moderate time to crystallize and therefore the crystal size are much smaller (see **Figure 3b**). Our GIWAXS

measurements in **Figure S2** confirm the varying structural order in these pure INPIC-4F films, although we were not able to analyze the CF-cast film due to the limited synchrotron beam time. The CB-cast INPIC-4F shows the strongest (100) edge-on lamellar diffraction ring at q_z=0.49 Å^{-1} (d=12.8 Å, obtained from d=$2\pi/q$) in the out-of-plane direction, together with diffraction peaks at q_z=1.2-1.6 Å^{-1} that we associate with the polycrystalline ordering of INPIC-4F. And When the casting solvent was changed to CB:CF (1.5:1, v/v) mixture, the intensity of the edge-on (100) diffraction ring reduced and the polycrystalline rings disappeared. Face-on (100) rings appeared in the in-plane direction, with the typical $\pi-\pi$ stacking (010) crescent appearing at q_z=1.83 Å^{-1} (d=3.4 Å) in the out-of-plane direction.

Figure S3a-c shows the optical microscopy images of PBDB-T:INPIC-4F blend films. It can be stated that the blend films are much smoother when cast using CF and CB:CF(1.5:1, v/v) mixture. Tapping-mode atomic force microscopy (AFM) of these films was applied to investigate the surface morphology of the photoactive layer as shown in **Figure 3d-f**. The root-mean-square (*RMS*) roughness of the blend film surfaces processed with CB, CB:CF and CF were 36.2, 4.1 and 2.2 nm, respectively. When CB was used as the casting solvent, the blend film showed INPIC-4F spherulites whose sizes ranged from 20 to 50 nm. Concurrently, the film cast from CB:CF (1.5:1, v/v) was uniform with continuous domains for efficient charge transport. The film cast from CF was smoother still, without obvious phase separation, a morphology that is beneficial for exciton dissociation but will be a disadvantage for charge transport towards electrodes because of the lack of adequate bi-continuous networks. These results suggest that reducing the molecular organization time using fast-evaporation solvents can efficiently hamper the overgrowth of INPIC-4F crystals and affect phase separation between donors and acceptors.

We continue to explore the molecular order in the blend films using GIWAXS measurements.[45-47] The 2D GIWAXS patterns of PBDB-T:INPIC-4F films cast from CB, CB:CF(1.5:1, v/v) and CF are shown in **Figure 4a-c,** and the 1D profiles in the out-of-plane direction are plotted in **Figure 4d**. Literature work has shown that PBTB-T has its (100) diffraction peak at q_z= 0.29 Å^{-1} (d=21.7 Å), and a $\pi-\pi$ stacking peak at q_z= 1.70 Å^{-1} (d=3.7 Å).[42] For the blend film cast from CB, the (100) diffraction peaks of PBDB-T and INPIC-4F both appear, at q_z= 0.29 and 0.49 Å^{-1} (d=21.7 and 12.8 Å), respectively. The polycrystalline peaks of INPIC-4F at q_z=1.2-1.6 Å^{-1} also appear, suggesting high crystallinity of INPIC-4F in the blend films, an

observation that is consistent with the existing of INPIC-4F spherulites shown in **Figure 4d**. When using CB:CF or CF as the casting solvent, the edge-on (100) diffraction rings of INPIC-4F disappeared, and broad diffraction peaks at q_z=1.4-2.0 Å^{-1} emerged, which is due to the convolution of $\pi-\pi$ stacking and polycrystalline rings of PBDB-T and INPIC-4F. We have therefore deconvoluted these broad diffraction peaks via multi-peak fitting with Gaussian peaks. **Figure 4e-g** shows the multi-peak fitting results of 1D profiles of PBDB-T:INPIC-4F films cast using different solvents. All these broad peaks can be deconvoluted into a polycrystalline INPIC-4F peak at q_z=1.56-1.58 Å^{-1}, and $\pi-\pi$ stacking peaks of PBDB-T and INPIC-4F at q_z=1.70 and 1.83Å^{-1} (d=3.7 and 3.4 Å), consistent with our own measurements as well as literature reports. The polycrystalline INPIC-4F peak is strongest in the CB-cast blend film, and becomes weaker when the casting solvent is CB:CF or CF. The $\pi-\pi$ stacking peak of PBDB-T is stronger in the CB-cast film, but the $\pi-\pi$ stacking peak of INPIC-4F is stronger in the CB:CF- and CF- cast films. We can conclude that in our best-performing devices cast from CB:CF, both PBDB-T and INPIC-4F are preferentially face-on $\pi-\pi$ stacked, which is beneficial for efficient exciton splitting at the donor/acceptor interfaces and facilitates efficient charge transport towards the electrode.
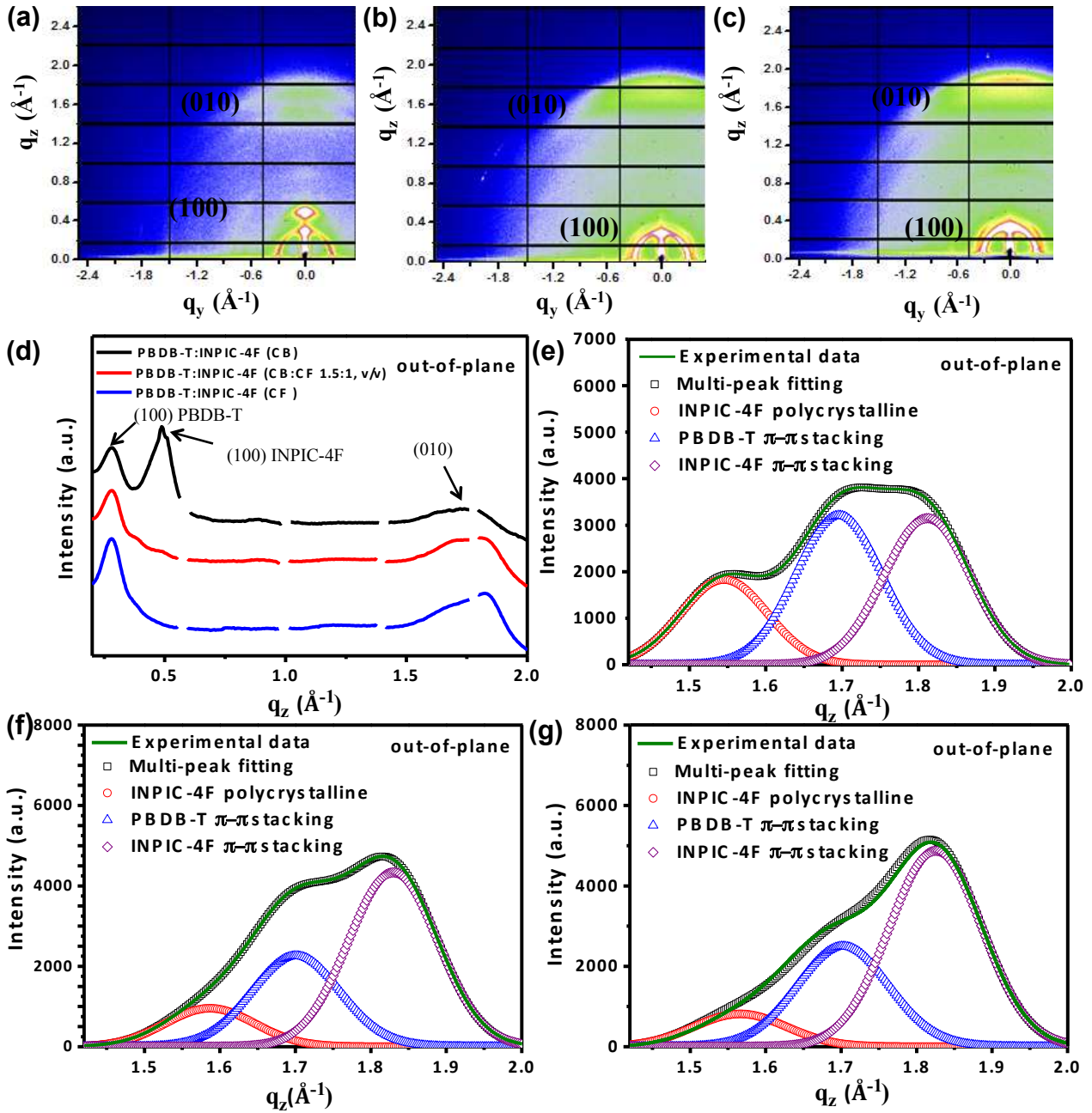
Figure 4 2D GIWAXS patterns of PBDB-T:INPIC-4F blend films prepared from (a) CB, (b) CB:CF (1.5:1, v/v) and (c) CF. Out-of-plane 1D profiles of GIWAXS patterns along the q_z axis of (d) PBDB-T:INPIC-4F films under different conditions. Multi-peak fitting results from 1.4 to 2.0Å^{-1} of PBDB-T:INPIC-4F films (e) CB, (f) CB:CF (1.5:1, v/v) and (g) CF.

The exciton dissociation and charge extraction processes are probed by analyzing the photocurrent (J_{ph}) versus effective voltage (V_{eff}) plots of various devices (**Figure 5** and **Table 2**). J_{ph} is defined as J_L- J_D, where J_L and J_D are the photocurrent densities under illumination and in the dark respectively. V_{eff} is defined as $V_{eff} = V_0 - V_a$, where V_0 is the voltage at the point of $J_{ph} = 0$ and V_a is the applied bias. Herein, the J_{ph} of PBDB-T:INPIC-4F based devices at 1 V reverse bias has

been selected as the pseudo saturation photocurrent (J_{sat}) for equitable comparison.[48] The J_{ph}/J_{sat} values under short-circuit and the maximal power output conditions represent the exciton dissociation efficiency (P_{diss}) and charge collection efficiency (P_{coll}), respectively. [49]It was found that the devices cast from CB:CF (1.5:1, v/v) have the highest J_{sat}, P_{diss} and P_{coll}, indicating that the solvent mixture helps enhance the efficiency of exciton generation, dissociation and charge collection.[50] Dark J-V curves of hole-only and electron-only devices are shown in **Figure S4** and the corresponding hole (μ_h) and electron (μ_e) mobilities are summarized in **Table 2**. The charge mobilities are generally described by the Mott-Gurney equation: $J = \frac{9}{8}\varepsilon_r\varepsilon_0\mu\frac{V^2}{L^3}$. where J is the current density, ε_0 is the permittivity of free space (8.85×10^{-14} F/cm), ε_r is the dielectric constant, μ is the charge mobility, V is the applied voltage and L is the thickness of the active layer. The ε_r parameter is assumed to be 3, which is a typical value for organic semiconductor.[51, 52] The μ_h and μ_e of the devices using CB or CF as solvent are $5.1\times10^{-4}/6.8\times10^{-4}$ cm^{2}V^{-1}S^{-1} and $5.2\times10^{-4}/6.8\times10^{-4}$ cm^{2}V^{-1}S^{-1}, respectively. These mobilities are similar and unbalanced, which will affect the performance of devices. When casting from CB:CF solvent mixture, the PBDB-T:INPIC-4F film exhibits higher and more balanced mobilities (μ_h=7.2×10^{-4} cm^{2}V^{-1}S^{-1}, μ_e=7.8×10^{-4} cm^{2}V^{-1}S^{-1}, μ_h /μ_e= 0.92), which is very beneficial to the improvement of J_{sc}.[53]

To gain more insight into the charge recombination process, we have evaluated the light intensity dependent V_{oc} changes. Light ideality factor ($n_{id,l}$) values were obtained by $n_{id,l} = \frac{q}{kT}\frac{dV_{oc}}{dln(\Phi)}$, where q is the electron charge, k is Boltzmann's constant, T is the absolute temperature, and Φ is the fractional light intensity normalized to 1 sun.[54] Previous work has shown that bimolecular recombination dominates the recombination process when the slope of the V_{oc} versus ln(P$_{light}$) plot is 1.00 kT/q. Alternatively, a slope larger than unity kT/q is a signature that monomolecular or trap-assisted recombination will operate.[55] The $n_{id,l}$ values of 1.26 (CB cast), 1.22 (CB:CF cast) and 1.28 (CF cast) were obtained respectively (see **Figure S5a**). Indeed, bimolecular recombination operates in all these devices while trap-assisted recombination is very weak. The $log(J_{sc})$ versus log(P_{light}) plots (**Figure S5b**) will give a slope of 1 if most of free carriers are swept out and collected by electrodes before recombination.[56] When using CB as the solvent, the slope is estimated to be 0.94, which affirms the inclination of strong bimolecular recombination and is responsible for low device J_{sc}. Slopes of 1 are determined in devices cast from CF and CB:CF mixture, indicating weak bimolecular recombination and efficient charge extraction.
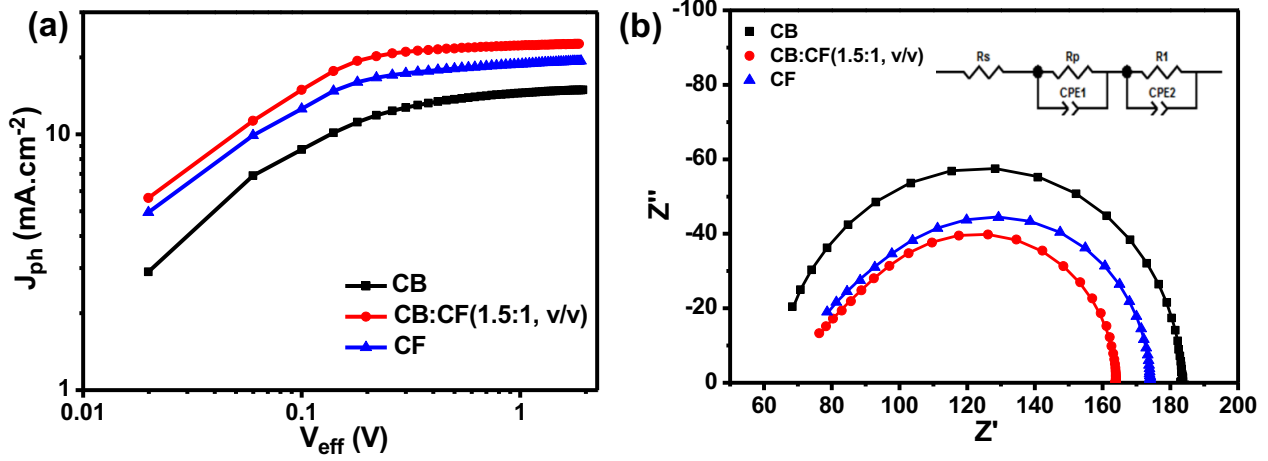
Figure 5 (a) Photocurrent density versus effective voltage curves of PBDB-T:INPIC-4F films cast from different solvents. (b) Nyquist plots of impedance spectra of various devices under 1 sun irradiation with an applied bias at V_{oc}.

Table 2 J_{sat}, P_{diss}, P_{coll}, hole and electron mobilities of PBDB-T:INPIC-4F OSCs prepared under different conditions.

Solvent	J_{sat} [mA cm^{-2}]	P_{diss} [%]	P_{coll} [%]	Hole mobility (μ_h) cm^{2}V^{-1}S^{-1}	Electron mobility (μ_e) cm^{2}V^{-1}S^{-1}	μ_h /μ_e
CB	14.9	97.9	86.3	5.1×10^{-4}	6.8×10^{-4}	0.75
CB:CF(1.5:1, v/v)	22.6	98.6	87.2	7.2×10^{-4}	7.8×10^{-4}	0.92
CF	19.4	98.4	85.6	5.2×10^{-4}	6.8×10^{-4}	0.76

Table 3 Summary of the electrical parameters of OSCs obtained by fitting the Nyquist plots.

Solvent	R_s [Ω]	R_p [Ω]	CPE_1-T [F]	R_1 [Ω]	CPE_2-T [F]
CB	64.2	108.5	1.28 E^{-8}	10.8	2.64 E^{-8}
CB:CF(1.5:1, v/v)	71.3	75.4	2.87 E^{-8}	19.4	3.98 E^{-8}
CF	74.3	83.4	1.83 E^{-8}	17.3	1.59 E^{-8}

Figure 5b shows the Nyquist plots of impedance measurements for these devices under different conditions, measured under a small voltage perturbation with an applied bias near open circuit voltage and under 0.1 sun irradiation. All devices exhibit a single semi-circle characteristic, therefore we applied an equivalent circuit model consisting of three resistances (R_s, R_p and R_1) and

two constant phase elements (*CPE₁-T, CPE₂-T*) to fit the curves.[57] Here, R_s corresponds to the series resistance of the device, which remains almost constant for all devices. R_p and *CPE₁-T* correspond to the resistance and capacitance of the photoactive layer. R_p of devices cast from CB, CF and CB:CF (1.5:1, v/v) are 108.5, 83.4, and 75.4 Ω, respectively. The decreasing contact resistance R_p leads to more efficient charge transport in the active layer. *CPE₁-T* is defined as the behavior of capacitor of the bulk photovoltaic layer. The increasing *CPE₁-T* implies an enriched interfacial area between PBDB-T and INPIC-4F. Generally, a larger interfacial area is beneficial to charge transport. R_1 refers to recombination resistance and is associated with two electrical contacts between the active layer and electrodes. For the CB-, CF-, and CB:CF- cast devices, R_1 increased from 10.8 to 17.3 and 19.4 Ω. This result suggests that CB:CF (1.5:1, v/v) helps reduce the recombination rate, which is consistent with our conclusions of V_{oc} and J_{sc} versus P_{light} of these devices. As described in previous work,[58] *CPE₂-T* is the capacitor associated with two electrical contacts between the active layer and electrodes. When CB:CF is the casting solvent, the *CPE₂-T* of all devices is highest, which indicates the reduced recombination and improved charge transport.

Conclusion

In summary, we have demonstrated a binary solvent approach to improve the efficiency of PBDB-T:INPIC-4F non-fullerene OSCs from 8.1% to 13.1%. Casting solvents with different boiling points change the film drying time, therefore can regulate the molecular ordering and optimize the phase separated nanoscale morphology within the photoactive layer. When the casting solvent is CB, the INPIC-4F acceptor will grow into large spherulites, leading to excessive phase separation with PBDB-T, which results in a rough active layer, weak absorption in the short wavelength region, inefficient exciton dissociation and poor charge transport properties. Conversely, casting from CF leads to a smooth active layer with small domains, reduced absorption in the long wavelength region and face-on π−π stacking of both PBDB-T and INPIC-4F. Encouragingly, when using the CB:CF (1.5:1, v/v) solvent mixture as the casting solvent, the absorption is strongest through the whole wavelength region. Meanwhile, both PBDB-T and INPIC-4F molecules are largely aligned with a face-on π-π stacking, which facilitate exciton dissociation and charge transport towards electrodes. As a result, the PBDB-T:INPIC-4F device cast from CB:CF (1.5:1, v/v) achieves a remarkable PCE_{max} of 13.1%. Our results build a fundamental understanding between the variations of molecular organization of donor and acceptor cast from different solvents and the

photovoltaic properties, which provides a rational guide for improving device efficiency of non-fullerene OSCs.

Experimental Section

Materials: INPIC-4F was synthesized according to our previous work.[37] PBDB-T was purchased from Solarmer Materials (Beijing) Inc. ZnO precursor solution was prepared by dissolving 0.2 g of zinc acetate dihydrate ($Zn(CH_3COO)_2.2H_2O$, 99.9%, Aladdin) and 0.056 mL ethanolamine ($NH_2CH_2CH_2OH$, 99.5%, Aladdin) in 2 mL of 2-methoxyethanol ($CH_3CH_2CH_2OH$, 99.8%, Aladdin).

Fabrication of polymer solar cells: All solar cells were fabricated in an inverted structure. The patterned ITO-glass substrates (resistance *ca.* 15 Ω per square) were cleaned by sequential sonication in water, ethanol, and isopropyl alcohol for 15 minutes each, before drying at 100 °C on a hotplate. These substrates were further treated with ultraviolet/ozone for 20 min before solution processing. The ZnO precursor solution was spin-coated at 4000 r.p.m on the ITO surface, then dried at 200 °C for 30 min in air. The photoactive layer was then deposited on top of the ZnO layer by spin-coating from a 14 mg/mL solution with 0.5 % DIO (volume ratio) of PBDB-T:INPIC-4F(1:1, weight ratio) to obtain films of 100 nm thickness, in a nitrogen-filled glovebox. After the casting of active layer, devices were further treated with thermal annealing at 100 °C for 10 min. Then 10 nm MoO_3 and 100 nm Ag were thermally evaporated forming the anode and counter electrode under high vacuum to finish the device preparation. The size of the photoactive area defined by the overlapping of anode and cathode is 4 mm^2.

Characterization: The HOMO and LUMO energy levels of donors and acceptors are calculated from the onset oxidation ($E_{onset,ox}$) and reduction potentials (E_{red}) from cyclic voltammetry measurements, and calibrated using ferrocene/ferrocenium ($E_{1/2, Fc/Fc+}$) according to the equation: $E_{HOMO/LUMO} = -(4.80 - E_{1/2,Fc/F_c^+} + E_{onset,ox/red,})$.[13] Film thickness was measured using a spectroscopic ellipsometer (J. A. Woollam, USA). The surface morphologies of films were characterized by optical microscope (Olympus, Japan), tapping-mode atomic force microscopy (AFM) (NT-MDT, Russia). Synchrotron based grazing incidence wide angle X-ray scattering (GIWAXS) measurements were conducted at beamline I07 of Diamond Light Source in UK. Film absorption spectra were measured using a UV-Visible spectrophotometer (HITACHI, Japan).

Photoluminescence (PL) was obtained using a PL microscopic spectrometer (Flex One, Zolix, China) with a 532 nm CW laser as the excitation source. Device J-V characterization was performed under AM 1.5G (100 mW cm^{-2}) using a Newport 3A solar simulator (USA) in air at room temperature. The light intensity was calibrated using a standard silicon reference cell certified by the National Renewable Energy Laboratory (NREL, USA). J-V characteristics were recorded using J-V sweep software developed by Ossila Ltd. (UK) and a Keithley 2612B (USA) source meter unit. External quantum efficiency (EQE) was measured with a Zolix (China) EQE system equipped with a standard Si diode. Impedance measurements were performed on an XM-studio electrochemical workstation (Solartron, U.K.).

Reference

(1)   Heeger AJ, *Chem. Soc. Rev*, **2010**, *39*: 2354-2371.

(2)   Heeger AJ, *Adv. Mater*, **2014**, *26*: 10-28.

(3)   Li W, Ye L, Li S, Yao H, Ade H, Hou J, *Adv. Mater*, **2018**, *30*: 1707170.

(4)   Zhou Y, Li M, Song J, Liu Y, Zhang J, Yang L, Zhang Z, Bo Z, Wang H, *Nano Energy*, **2018**, *45*: 10-20.

(5)   Zhang J, Yan C, Wang W, Xiao Y, Lu X, Barlow S, Parker TC, Zhan X, Marder SR, *Chem. Mater,* **2018**, *30*: 309-313.

(6)   Luo Z, Bin H, Liu T, Zhang Z, Yang Y, Zhong C, Qiu B, Li G, Gao W, Xie D, Wu K, Sun Y, Liu B, Li Y, Yang C, *Adv. Mater*, **2018**, *30*: 1706124.

(7)   Li C, Xie Y, Fan B, Han G, Yi Y., Sun Y, *J. Mater. Chem. C*, **2018**, *6*: 4873-4877.

(8) Fan B, Zhang D, Li M, Zhong W, Zhao Z, Ying L, Huang F, Cao Y. *Sci China Chem*, **2019**, *62*: 1-7.

(9) Nielsen CB, Holliday S, Chen H, Cryer SJ, McCulloch I, *Acc. Chem. Res*, **2015**, *48*: 2803-2812.

(10) Lin Y, Wang J, Dai S, Li Y, Zhu D, Zhan X, *Adv. Energy Mater*, **2014**, *4*: 1400420.

(11) Li S, Ye L, Zhao W, Liu X, Zhu J, Ade H, Hou J, *Adv. Mater*, **2017**, *29*: 1704051.

(12) Lopez SA, Sanchez-Lengeling B, De Goes Soares J, Aspuru-Guzik A, *Joule* , **2017**, *1*: 857-870.

(13) Cui Y, Zhang S, Liang N, Kong J, Yang C, Yao H, Ma L, Hou J, *Adv. Mater*, **2018**, *30*: 1802499.

(14) Zhang Z, Feng L, Xu S, Liu Y, Peng H, Zhang Z, Li Y, Zou Y, *Adv. Sci*, **2017**, *4*: 1700152.

(15) Lin Y, Wang J, Zhang Z, Bai H, Li Y, Zhu D, Zhan X, *Adv. Mater*, **2015**, *27*:1170-1174.

(16) Zhao W, Qian D, Zhang S, Li S, Inganäs O, Gao F, Hou J, *Adv. Mater*, **2016**, *28*: 4734–4739.

(17) Min J, Cui C, Heumueller T, Fladischer S, Cheng X, Spiecker E, Li Y, Brabec CJ, *Adv. Energy Mater*, **2016**, *6*: 1600515.

(18) Chao P, Wang H, Qu S, Mo D, Meng H, Chen W, He F, *Macromolecules*, **2017**, *50*: 9617-9625.

(19) Wu Y, An C, Shi L, Yang L, Qin Y, Liang N, He C, Wang Z, Hou J, *Angew. Chemie - Int. Ed*, **2018**, *57*: 12911-12915.

(20) Tang L, Xiao J, Bai W, Li Q, Wang H, Miao M, Yip H, Xu Y, *Org. Electron*, **2019**, *64*: 1-6.

(21) Chen H, Hou J, Zhang S, Liang Y, Yang G, Yang Y, Yu L, Wu Y, Li G, *Nat. Photonics*, **2009**, *3*: 649-653.

(22) Fan Q, Wang Y, Zhan M, Wu B, Guo X, Jiang Y, Li W, Guo B, Ye C, Su W, Fang J, Ou X, Liu F, Wei Z, Sum T. C, Russell TP, Li Y, *Adv. Mater*, **2018**, *3:*1704546.

(23) Ke X, Kan B, Wan X, Wang Y, Zhang Y, Li C, Chen Y, *Dye. Pigment*, **2018**, *155*: 241-248.

(24) Kini GP, Choi JY, Jeon SJ, Suh IS, Moon DK, *Polymer* , **2018**, *148*: 330-338.

(25) Zhao F, Dai S, Wu Y, Zhang Q, Wang J, Jiang L, Ling Q, Wei Z, Ma W, You W, Wang C, Zhan X, *Adv. Mater*, **2017**, *29*: 1700144.

(26) Zhang Q, Kelly M. A, Bauer N, You W *Acc. Chem. Res*, **2017**, *50*: 2401-2409.

(27) Dai S, Zhao F, Zhang Q, Lau TK, Li T, Liu K, Ling Q, Wang C, Lu X, You W, Zhan X, *J. Am. Chem. Soc*, **2017**, *139*: 1336-1343.

(28) Zhang Y, Yao H, Zhang S, Qin Y, Zhang J, Yang L, Li W, Wei Z, Gao. F, Hou J, *Sci. China Chem*, **2018**, *61*: 1328-1337.

(29) Zhao W, Li S, Yao H, Zhang S, Zhang Y, Yang B, Hou.J, *J. Am. Chem. Soc*, **2017**, *139*: 7148-7151.

(30) Fan Q, Su W, Wang Y, Guo B, Jiang Y, Guo X, Liu F, Russell TP, Zhang M, Li Y, *Sci. China Chem*, **2018**, *61*: 531-537.

(31) Yao H, Cui Y, Yu R, Gao B, Zhang H, Hou J, *Angew. Chemie - Int. Ed*, **2017**, *56*: 3045-3049.

(32) Yao H, Chen Y, Qin Y, Yu R, Cui Y, Yang B, Li S, Zhang K, Hou J, *Adv. Mater*, **2016**, 8283-8287.

(33) Song X, Gasparini N, Ye L, Yao H, Hou J, Ade H, Baran D, *ACS Energy Lett*, **2018**, *3*: 669-676.

(34) Guo X, Zhang M, Ma W, Y. L, Zhang S, Liu S, Ade H, Huang F, Hou J, *Adv. Mater*, **2014**, *26*: 4043-4049.

(35) Guo X, Cui C, Zhang M, Huo L, Huang Y, Hou J, Li Y, *Energy Environ. Sci*. **2012**, *5*, 7943-7949

(36) Q Wan, X Guo, Z Wang, W Li, B Guo, W Ma, M Zhang, Y Li, *Adv. Funct. Mater*, **2016**, *26*: 6635-6640.

(37) Guo X, Zhang M, Ma W, Zhang S, Hou J, Li. Y, *RCS Adv*, **2016**, *6*: 51924-51931.

(38) Ye L, Zhang S, Ma W, Fan B, Guo X, Huang Y, Ade H, Hou J, *Adv. Mater*, **2012**, *24*: 6335-6341.

(39) Yao Y, Ho. J, Xu Z, Li G, Yang Y, *Adv. Funct. Mater*, **2008**, *18*: 1783-1789.

(40) Qian D, Ye L, Zhan. M, Liang Y, Li L, Huang Y, Guo X, Zhang S, Tan Z., Hou J, *Macromolecules*, **2012**, *45*: 9611-9617.

(41) Wu H, Fan H, Xu S, Zhang C, Chen S, Yang C, Chen D, Li. F, Zhu X, *Sol. RRL*, **2017**, *1*:1700165.

(42) Sun J, Ma X, Zhang Z, Yu.J, Zhou J, Yin X, Yang L, Geng R, Zhu R, Zhang F, Tang W, *Adv. Mater*, **2018**, *30*: 1707150.

(43) Li W, Cai J, Yan Y, Cai. F, McGettrick JD, Watson TM, Li Z, Pearson AJ, Lidzey DG, Hou J, Wang T, *Sol. RRL*, **2018**, *2*: 1800114.

(44) Li W, Chen M, Zhang Z, Cai J, Zhang H, Gurney RS, Liu D, Yu J, Tang W, Wang T, *Adv.*

Funct. Mater, **2019**, *29*: 1807662.

(45)   Müller-Buschbaum P, *Adv. Mater*, **2014**, *26*: 7692-7709.

(46)   Lee J, Ko SJ, Seifri. M, Lee H, McDowell C, Luginbuhl BR, Karki A, Cho K, Nguyen TQ, Bazan GC, *Adv. Energy Mater*, **2018**, *8*: 1801209.

(47)   Yang J, Uddin MA, Tang Y, WangY, Su H, Gao R Chen K, Dai J, Woo HY Guo X, *ACS Appl. Mater. Interfaces*, **2018**, *10*: 23235-23246.

(48)   Li W, Cai J, Cai F,Yan Y, Yi H, Gurney RS, Liu D, Iraqi A, Wang T, *Nano Energy*, **2018**, *44*: 155-163.

(49)   He Z, Zhong C, Huang X, Wong W, Wu H, Chen L, Su S, Cao Y. *Adv Mater*, **2011**, *23*:4636–4643.

(50)   Xie Y, Zhou W, Yin J, Hu X, Zhang L, Meng X, Ai Q, Chen Y, *J. Mater. Chem. A*, **2016**, *4*: 6158-6166.

(51)   An Q, Zhang F, Gao W, Sun Q, Zhang M, Yang C, Zhang J, *Nano Energy*, **2018**, *45*: 177-183.

(52)   Guo X, Zhang M, Tan J, Zhang S, Huo L, Hu W, Li Y, Hou J, *Adv. Mater*, **2012**, *24*: 6536-6541.

(53)   Li W, Yan Y, Gong Y, Cai J, Cai F, Gurney RS, Liu D, Pearson AJ, Lidzey DG, Wang T, *Adv. Funct. Mater*, **2018**, *28*: 1704212.

(54)   Koster LJA, Mihailetchi VD, Xie H, Blom PWM, *Appl. Phys. Lett*, **2005**, *87*: 203502.

(55)   Ye L, Xie Y, Weng K, Ryu HS, Li C, Cai Y, Fu H, Wei D, Woo HY, Tan S, Sun Y, *Nano Energy*, **2019**, *58*: 220-226.

(56)   Kan B, Zhang J, Liu F, Wan X, Li C, Ke X, Wang Y, Feng H, Zhang Y, Long G, Friend RH, Bakulin AA, Chen Y, *Adv. Mater*, **2018**, *30*: 1704904.

(57)   Zheng Y, Goh T, Fan P, Shi W, Yu J, Taylor AD, *ACS Appl. Mater. Interfaces*, **2016**, *8*: 15724-15731.

(58)   Xiao B, Zhang M, Yan J, Luo G, Gao K, Liu J, You Q, Wang HB, Gao C, Zhao B, Zhao X, Wu H, Liu F, *Nano Energy*, **2017**, *39*: 478-488.

Table of Contents Entry